V European Conference on Computational Fluid Dynamics
ECCOMAS CFD 2010
J. C. F. Pereira and A. Sequeira (Eds)
Lisbon, Portugal,14-17 June 2010

MONOTONE NONLINEAR SCHEME FOR VARIABLE DENSITY GROUNDWATER FLOW

Dragan Vidović*, Milenko Pušić†

*Institute "Jaroslav Černi",
Belgrade, Serbia
e-mail: draganvid@gmail.com
†Faculty For Mining And Geology
Belgrade, Serbia
e-mail: mpusic@ptt.rs

Key words: Nonlinear diffusion, groundwater, finite volume, buoyancy

Abstract. *Permeability of ground is a discontinuous anisotropic quantity that may change abruptly several orders of magnitude between geological layers. In combination with the mesh distortion, this presents a major difficulty for numerical modeling. Standard linear finite element method is not monotone and may produce unphysical oscillations, while the classical finite volume two-point flux approximation is monotone but not even first order accurate on distorted meshes.*

Recently a new class of nonlinear finite volume methods for diffusion appeared in [17] and was further developed in [15, 18, 20, 13, 7, 14]. These methods compute a two-point diffusive flux approximation in a non-linear iterative fashion, resulting in a solution which is monotone and second-order accurate.

In this paper we extend the method presented in [13] to the variable density flow in three dimensions. In addition to the groundwater flow equation formulated in terms of pressure and buoyancy, a convection-diffusion equation is solved for concentration. Iterative procedure to determine the coefficients of the nonlinear diffusive flux approximation is performed together with Picard iterations for the convective term.

In order to demonstrate the monotonicity and the accuracy of the scheme, we present results obtained for Elder problem, and for a problem of mixing trough an interface.

1 INTRODUCTION

Discontinuous anisotropic hydraulic permeability of ground presents a difficulty for numerical computations. Classical methods usually deployed for groundwater flow computations sometimes exhibit unphysical oscillations or hampered convergence, especially if ground parameters change greatly and abruptly.

Finite difference method gives good results, but requires structured meshes, which had triggered the development of methods for unstructured meshes.

The most popular linear variant of the finite element method [5], as well as the mixed finite element method [3], are not monotone on arbitrary unstructured meshes [11]. The same holds for the Discontinuous Galerkin methods [6, 2]. The lack of monotonicity may lead to non-physical oscillatory solutions.

Classical linear two-point finite volume approximation of diffusive fluxes is monotone, but not even first-order accurate on arbitrary meshes [13]. Finite volume methods with higher-order linear multipoint flux approximations are not monotone, and may lead to oscillatory solutions.

To address this problem, a class of non-linear monotone finite volume methods has been developed in [17, 15, 18, 20, 13, 7, 14].

In this paper we present a scheme for the computation of groundwater flow with variable density. We use the nonlinear method described in [13] to compute diffusive mass fluxes, as well as the fluxes in the pressure equation, while the advective mass fluxes are computed using a full upwind finite volume discretization.

The accuracy of the scheme is tested for Elder problem, and for a problem of mixing trough an interface.

2 EQUATIONS OF GROUNDWATER FLOW WITH MASS TRANSPORT

In this paper we adopt Boussinesq approximation and neglect the effects of water and ground compressibility, which together with the absence of free water surface (water table) leads to instantaneous pressure propagation trough the domain. Transient character of the problem comes from the concentration equation. Equations modeling such physical system are the following:

$$\mathbf{u} = -\frac{\boldsymbol{\kappa}}{\mu}\left(\nabla p - \rho \mathbf{g}\right), \tag{1}$$

$$\nabla \cdot \mathbf{u} = 0, \tag{2}$$

$$\frac{\partial(\varepsilon c)}{\partial t} + \nabla \cdot (\mathbf{u}c - \varepsilon D \nabla c) = 0, \tag{3}$$

$$\rho = \rho(c), \tag{4}$$

where $\mathbf{u}$ is the Darcy velocity, $\boldsymbol{\kappa}$ is the permeability tensor, μ is the dynamic viscosity, p is the pressure, ρ is the solute density, $\mathbf{g} = [0, 0, -g]^T$ is a gravity vector, g is the acceleration due to gravity, ε is the medium porosity, c is the concentration, and D is the

sum of the diffusion and the dispersion coefficients. Equation (1) represents Darcy's law, (2) is the incompressibility condition, (3) is the advection-dispersion equation for porous media, and (4) is the equation of state.

For this system to have a unique solution, boundary conditions must be prescribed, as well as the initial conditions for c. It is assumed that in each point of the domain boundary either Dirichlet or Neumann condition is prescribed for each variable, and that Neumann condition may not be prescribed for the concentration at inflow boundaries.

3 DISCRETIZATION

3.1 Collocation points

Method presented in [13] requires that $\boldsymbol{\kappa}/\mu$ is constant by parts, changing only across the interfaces between cells, and at most across one interface of any cell. These limitations have been softened in [7], where $\boldsymbol{\kappa}/\mu$ may jump over more than one face of a cell, and may also vary moderately within cells. Our implementation is based on [13], and we shall assume that the corresponding limitations are hold. We shall refer to the areas of constant $\boldsymbol{\kappa}/\mu$ as *permeability zones*.

Porosity ε could jump between layers, although not as much as the permeability, so the effective diffusion coefficient εD appearing in (3) could be discontinuous. For the matter of simplicity we assume that this is not the case.

For each variable (i.e. for the pressure and for the concentration), one collocation point is assigned to each cell and to each boundary face. In addition, one collocation point for the pressure is assigned to each face over which $\boldsymbol{\kappa}/\mu$ jumps. The face collocation points are introduced only for mathematical convenience and do not enter the final algebraic system.

Pressure and concentration collocation points are denoted by $\mathbf{x}^p_\Omega$ and $\mathbf{x}^c_\Omega$, respectively, in cell Ω, or by $\mathbf{x}^p_f$ and $\mathbf{x}^c_f$ in face f. Boundary collocation points are taken to be face centroids. Concentration cell collocation points are taken to be cell centroids. If Ω_+ and Ω_- are two cells sharing face f and $\boldsymbol{\kappa}/\mu$ jumps between these cells, then $\mathbf{x}^p_{\Omega_+}$, $\mathbf{x}^p_{\Omega_-}$ and $\mathbf{x}^p_f$ are determined such that

$$(\mathbf{x}^p_f - \mathbf{x}^p_{\Omega_+}) \times \boldsymbol{\ell}_+ = 0, \qquad (\mathbf{x}^p_f - \mathbf{x}^p_{\Omega_-}) \times \boldsymbol{\ell}_- = 0, \tag{5}$$

as proposed in [13], where $\ell_\pm = (\boldsymbol{\kappa}/\mu)_{\Omega_\pm}\mathbf{n}_f$. All other pressure cell collocation points are centroids.

3.2 Pressure equation

Integrating (2) over polygonal control volume Ω and using the divergence theorem we arrive to

$$\sum_{f\in\partial\Omega} \chi_{\Omega,f} u_f = 0, \qquad u_f = \int_f \mathbf{u}\cdot\mathbf{n}_f ds, \tag{6}$$

where u_f is the normal flux trough face f, $\mathbf{n}_f$ is a unit vector normal to face f fixed once and for all, and $\chi_{\Omega,f} = 1$ if $\mathbf{n}_f$ is pointing outside of Ω, or -1 otherwise. For a single cell, we always assume that $\mathbf{n}_f$ is pointing outside. At boundary faces, fixed normal vectors are pointing outside.

Let us first assume that $\boldsymbol{\kappa}/\mu$ does not change across face f. Let $\boldsymbol{\ell}_f = (\boldsymbol{\kappa}/\mu)_f \mathbf{n}_f$. Using this notation, the definition of the directional derivative

$$\frac{\partial p}{\partial \boldsymbol{\ell}_f} = \nabla p \cdot \frac{\boldsymbol{\ell}_f}{|\boldsymbol{\ell}_f|}, \tag{7}$$

and Darcy's law (1), definition of u_f in (6) becomes

$$u_f = \int_f -\boldsymbol{\ell}_f \cdot (\nabla p - \rho \mathbf{g}) ds = -|\boldsymbol{\ell}_f| \int_f \frac{\partial p}{\partial \boldsymbol{\ell}_f} ds + \int_f \rho \mathbf{g} \cdot \boldsymbol{\ell}_f ds. \tag{8}$$

Among all pressure collocation points in faces adjacent to cell Ω or in the neighboring cells within the same permeability zone , three points $\mathbf{x}^1$, $\mathbf{x}^2$, and $\mathbf{x}^3$ are chosen such that

$$\frac{\boldsymbol{\ell}_f}{|\boldsymbol{\ell}_f|} = \alpha \frac{\mathbf{t}^1}{|\mathbf{t}^1|} + \beta \frac{\mathbf{t}^2}{|\mathbf{t}^2|} + \gamma \frac{\mathbf{t}^3}{|\mathbf{t}^3|}, \qquad \alpha \geq 0, \beta \geq 0, \gamma \geq 0, \tag{9}$$

where $\mathbf{t}^k = \mathbf{x}^k - \mathbf{x}_\Omega$. If such points cannot be found in the immediate neighborhood, the search is extended to the neighbors of the neighbors.

Using this decomposition, the first integral in (8) is written as

$$\begin{aligned} -|\boldsymbol{\ell}_f| \int_f \frac{\partial p}{\partial \boldsymbol{\ell}_f} ds = -|\boldsymbol{\ell}_f| \int_f \alpha \frac{\partial p}{\partial \mathbf{t}^1} + \beta \frac{\partial p}{\partial \mathbf{t}^2} + \gamma \frac{\partial p}{\partial \mathbf{t}^3} ds \approx \\ \approx -|\boldsymbol{\ell}_f||f| \left(\frac{\alpha}{|\mathbf{t}^1|}(p^1_\Omega - p_\Omega) + \frac{\beta}{|\mathbf{t}^2|}(p^2_\Omega - p_\Omega) + \frac{\gamma}{|\mathbf{t}^3|}(p^3_\Omega - p_\Omega) \right), \end{aligned} \tag{10}$$

where p^k_Ω is the pressure in $\mathbf{x}^k$, and p_Ω is the pressure in $\mathbf{x}_\Omega$. Let cells Ω_+ and Ω_- have a common edge f, and let us assume that $\mathbf{n}_f$ is pointing from Ω_+ to Ω_-. Approximations (10) corresponding to these two cells are linearly combined, omitting Ω in subscripts:

$$\begin{aligned} -|\boldsymbol{\ell}_f| \int_f \frac{\partial p}{\partial \boldsymbol{\ell}_f} ds \approx -A_+ |\boldsymbol{\ell}_f||f| \left(\frac{\alpha_+}{|\mathbf{t}^1_+|}(p^1_+ - p_+) + \frac{\beta_+}{|\mathbf{t}^2_+|}(p^2_+ - p_+) + \frac{\gamma_+}{|\mathbf{t}^3_+|}(p^3_+ - p_+) \right) \\ + A_- |\boldsymbol{\ell}_f||f| \left(\frac{\alpha_-}{|\mathbf{t}^1_-|}(p^1_- - p_-) + \frac{\beta_-}{|\mathbf{t}^2_-|}(p^2_- - p_-) + \frac{\gamma_-}{|\mathbf{t}^3_-|}(p^3_- - p_-) \right). \end{aligned} \tag{11}$$

For this approximation to be valid, it is required that

$$A_+ + A_- = 1. \tag{12}$$

In order to arrive at a two point formula, we choose A_+ and A_- such that the contributions of pressures other than p_+ and p_- in (11) cancel. This means that

$$-A_+ d_+ + A_- d_- = 0, \qquad d_\pm = \frac{\alpha_\pm}{|\mathbf{t}^1_\pm|} p^1_\pm + \frac{\beta_\pm}{|\mathbf{t}^2_\pm|} p^2_\pm + \frac{\gamma_\pm}{|\mathbf{t}^3_\pm|} p^3_\pm. \tag{13}$$

It may happen that $\mathbf{x}^k_-$ and $\mathbf{x}_+$ coincide, or that $\mathbf{x}^k_+$ and $\mathbf{x}_-$ coincide. In this case, the terms to be canceled and $d_\pm$ change. Note that $d_\pm \geq 0$ as long as $p \geq 0$.

If $d_+ + d_- > 0$, equations (12) and (13) determine coefficients

$$A_+ = \frac{d_-}{d_+ + d_-}, \qquad A_- = \frac{d_-}{d_+ + d_-}, \tag{14}$$

otherwise we set $d_\pm = \frac{1}{2}$.

In this way, the first integral in (8) is approximated using two-point formula

$$-|\boldsymbol{\ell}_f| \int_f \frac{\partial p}{\partial \boldsymbol{\ell}_f} ds \approx M^+_f p_+ - M^-_f p_-, \tag{15}$$

$$M^\pm_f = A_\pm |\boldsymbol{\ell}_f| |f| \left(\frac{\alpha_\pm}{|\mathbf{t}^1_\pm|} + \frac{\beta_\pm}{|\mathbf{t}^2_\pm|} + \frac{\gamma_\pm}{|\mathbf{t}^3_\pm|} \right), \tag{16}$$

where non-negative coefficients $M^\pm_f$ depending on p are determined iteratively.

If f is a boundary face, it is treated as a cell of zero volume, and formula (15) still holds, where p_- is the boundary pressure. If the pressure has not been prescribed in face f, it is computed using formulas (8), (15), and the prescribed flux.

The second integral in (8) is approximated as

$$\int_f \rho \mathbf{g} \cdot \boldsymbol{\ell}_f ds \approx |f| \rho_f \mathbf{g} \cdot \boldsymbol{\ell}_f. \tag{17}$$

If f is an internal face, density ρ_f is computed as volume average

$$\rho_f = \frac{|\Omega_+| \rho_+ + |\Omega_-| \rho_-}{|\Omega_+| + |\Omega_-|}, \tag{18}$$

where $\rho_\pm$ are the densities in $\Omega_\pm$ which are computed from concentrations $c_\pm$ using the equation of state (4). If f is a boundary face, ρ_f is computed using (4) from the boundary concentration, which may be prescribed, or computed during the concentration diffusive flux computation, in the same way the boundary pressures are computed (see Sec. 3.3).

If $\boldsymbol{\kappa}/\mu$ changes across face f, then let $\boldsymbol{\ell}_\pm = \mp (\boldsymbol{\kappa}/\mu)_\pm \mathbf{n}_f$. Instead of (8) we have

$$u_f = \pm |\boldsymbol{\ell}_\pm| \int_f \frac{\partial p}{\partial \boldsymbol{\ell}_\pm} ds \mp \int_f \rho \mathbf{g} \cdot \boldsymbol{\ell}_\pm ds. \tag{19}$$

Since in this case $\boldsymbol{\ell}_\pm = -|\boldsymbol{\ell}_\pm|(\mathbf{x}_f - \mathbf{x}_\pm)/|\mathbf{x}_f - \mathbf{x}_\pm|$ because of (5), directional derivatives can be well approximated using a two-point formula. Together with (17) this gives

$$u_f \approx \mp \frac{|f||\boldsymbol{\ell}_\pm|}{|\mathbf{x}_f - \mathbf{x}_\pm|} \left[p_f - p_\pm - \rho_\pm \mathbf{g} \cdot (\mathbf{x}_f - \mathbf{x}_\pm) \right]. \tag{20}$$

Continuity of flux at face f and formula (20) give a linear relation for pressure p_f

$$\frac{|\boldsymbol{\ell}_+|}{|\mathbf{x}_f - \mathbf{x}_+|} \left[p_f - p_+ - \rho_+ \mathbf{g} \cdot (\mathbf{x}_f - \mathbf{x}_+) \right] + \frac{|\boldsymbol{\ell}_-|}{|\mathbf{x}_f - \mathbf{x}_-|} \left[p_f - p_- - \rho_- \mathbf{g} \cdot (\mathbf{x}_f - \mathbf{x}_-) \right] = 0. \tag{21}$$

Calculating p_f from (21) and substituting it in (20) gives a two-point formula for the flux

$$u_f \approx \frac{|\boldsymbol{\ell}_+||\boldsymbol{\ell}_-|}{|\boldsymbol{\ell}_+||\mathbf{x}_f - \mathbf{x}_-| + |\boldsymbol{\ell}_-||\mathbf{x}_f - \mathbf{x}_+|} \left[p_+ - p_- + \rho_+ \mathbf{g} \cdot (\mathbf{x}_f - \mathbf{x}_+) - \rho_- \mathbf{g} \cdot (\mathbf{x}_f - \mathbf{x}_-) \right]. \tag{22}$$

3.3 Concentration equation

Equation (3) is integrated over control volume Ω and the divergence theorem is applied, resulting in

$$\int_\Omega \frac{\partial(\varepsilon c)}{\partial t} dt + \sum_{f \in \partial\Omega} \chi_{\Omega,f} \left[u_f c_f - |f| \left(\varepsilon D \frac{\partial c}{\partial n_f} \right)_f \right] = 0 \tag{23}$$

The diffusive-dispersive flux $-|f| \left(\varepsilon D \frac{\partial c}{\partial n_f} \right)_f$ is discretized in the same way as in the pressure equation, except that the situation is somewhat simpler because εD is assumed to be a scalar, and there is no gravity term.

It is essential to preserve the monotonicity of the scheme, otherwise concentrations may become negative, and then the nonlinear discretization of the diffusive term will break. Except at Dirichlet concentration boundaries, face concentration c_f appearing in the convective flux is resolved using the first order upwind discretization. If $\mathbf{n}_f$ is pointing from Ω_+ to Ω_-, then

$$c_f = \frac{1}{2}(u_f + |u_f|)c_+ + \frac{1}{2}(u_f - |u_f|)c_-. \tag{24}$$

In this way it is guaranteed that the scheme is monotone and therefore the concentration will not become negative. A less diffusive solution would be obtained using a second order limited scheme, like the one that appears in [14].

Euler implicit time discretization is used. The diffusive-dispersive term is evaluated implicitly at time level $n+1$. The convective term is linearized using Picard linearization, which means that flux u_f is evaluated explicitly, while the concentration is evaluated

implicitly. The discretized concentration equation now reads

$$\varepsilon_\Omega \frac{c_\Omega^{n+1,m+1} - c_\Omega^n}{\Delta t} + \sum_{f \in \partial\Omega} \chi_{\Omega,f} \left[u_f^{n+1,m} c_f^{n+1,m+1} + \right.$$
$$\left. + N_f^+(c^{n+1,m}) c_+^{n+1,m+1} - N_f^-(c^{n+1,m}) c_-^{n+1,m+1} \right] = 0, \tag{25}$$

where $\Delta t = t^{n+1} - t^n$ is the time step, $N_f^\pm$ are the concentration analogues of coefficients $M_f^\pm$ defined in (16), the first superscript denotes the time level, and the second superscript denotes the iteration number. Lack of the second superscript means that the last iteration is used. Cell and face concentrations and pressures obtained at the end of one time level are taken to be the initial values for iterations in the next time level. The whole procedure is summarized in Algorithm 1.

Algorithm 1 Solution procedure

```
Find all collocation points
Find all reconstruction vectors (9)
t = t_0,    n = 0
while t < t_end do
  m = 0
  repeat
    Compute ρ^{n+1,m} from c^{n+1,m}
    Compute p^{n+1,m+1} using (6), (8), (15), (17), (22), and the latest ρ
    Compute the fluxes using (8), (15), (17), (22), and the latest ρ
    Compute c^{n+1,m+1} from (25)
    m = m + 1
  until max(|p^{n+1,m+1} − p^{n+1,m}|) ≤ ε_inner ‖ p^{n+1,m+1} ‖_2 and
        max(|c^{n+1,m+1} − c^{n+1,m}|) ≤ ε_inner ‖ c^{n+1,m+1} ‖_2
  t = t + Δt,    n = n + 1
end while
```

4 EXAMPLES

The accuracy of the non-linear diffusion scheme was tested in [13]. This scheme is second order accurate in primary variables and first order accurate in fluxes. The upwind scheme used for the convective term is first order accurate.

We present two examples. The first example demonstrates that our scheme is far more accurate than if the classical linear two-point fluxes are used. The second example demonstrates that the results are similar to those obtained with another unstructured upwind scheme, and that the scheme behaves well in the presence of discontinuities in the material parameters and the solution.

Example 1. Constant Darcy velocity field of $2 \cdot 10^{-5}$m/s in x direction is specified in a unit cube by prescribing the appropriate initial pressure field, Dirichlet pressure boundary condition at the inflow, and Neumann pressure boundary condition at all other boundaries. We have chosen $K = \kappa\rho g/\mu = 10^{-4}$m/s, $\rho = 999.13$kg/m^3, $\varepsilon = 0.1$, $D = 2 \cdot 10^{-6}$m^2/s, and $\mu = 1.307e^{-3}$kg/(s $\cdot$ m). Density variations are neglected in this example.

Concentration

$$c = \begin{cases} 1.5\text{kg/m}^3, & z < 0.5 \\ 6.0\text{kg/m}^3, & z \geq 0.5 \end{cases} \tag{26}$$

is prescribed at all boundaries except at the outflow, and also as the initial condition. Zero diffusive flux is prescribed as the outflow concentration boundary condition.

Structured computational grid was obtained by subdividing each cube of a $32 \times 32 \times 32$ Cartesian grid into six tetrahedra. Computations were performed until the stationary solution was reached. Fig. 1 shows the concentration isolines at the outflow boundary. Image on the left shows the result obtained by the method presented in this paper, while the other image shows the result obtained by a modified method in which instead of (15) one uses the classical linear two-point flux formula

$$-|\boldsymbol{\ell}_f| \int_f \frac{\partial p}{\partial \boldsymbol{\ell}_f} ds \approx |\boldsymbol{\ell}_f||f| \frac{p_+ - p_-}{|\mathbf{x}_+ - \mathbf{x}_-|}. \tag{27}$$

Such linear two-point foruma is also used for the concentration diffusive flux in the second image. Due to the orientation of the grid, the error of the classical finite volume discretization accumulates, and causes the asymmetry visible in the image on the right. Such asymmetry is not visible in the result obtained by the non-linear method. The inaccuraces near the Dirichlet borders are due to post-processing.

This demonstrates that in spite of the fact that the convection discretization is only first order accurate, deployment of the non-linear diffusion discretization greatly improves the accuracy, because the large error of the classical method is mostly due to the inaccurate discretization of the pressure equation.

Example 2. Elder problem is a classical example of density driven flow. It was originally formulated for thermal convection in [9, 10] and reformulated for concentration-dependent density in [19]. It describes an unstable situation when dense fluid is placed above a lighter fluid. This causes onset of brines, also known ad "fingers". The geometry of the problem is shown in Fig. 2. Concentration $c = 1$ is prescribed along the central 300m of the upper boundary, and $c = 0$ along the lower boundary. On other boundaries concentration flux is zero. As a pressure boundary condition, zero flux was prescribed everywhere except in the upper two corners, where the atmospheric pressure is set. Maximal density is 1200kg/m^3, and minimal density is 1000kg/m^3. We assume that the density depends linearly on the concentration. Initial concentration is zero, and the initial pressure linearly increases with depth, so that the fluid does not move. Other data are $\kappa = 4.845 \cdot 10^{-13}$m^2, $\mu = 10^{-3}$kg/(s $\cdot$ m), $\varepsilon = 0.1$, $g = 9.81$m/s^2, and $D = 3.565 \cdot 10^{-6}$m^2/s.

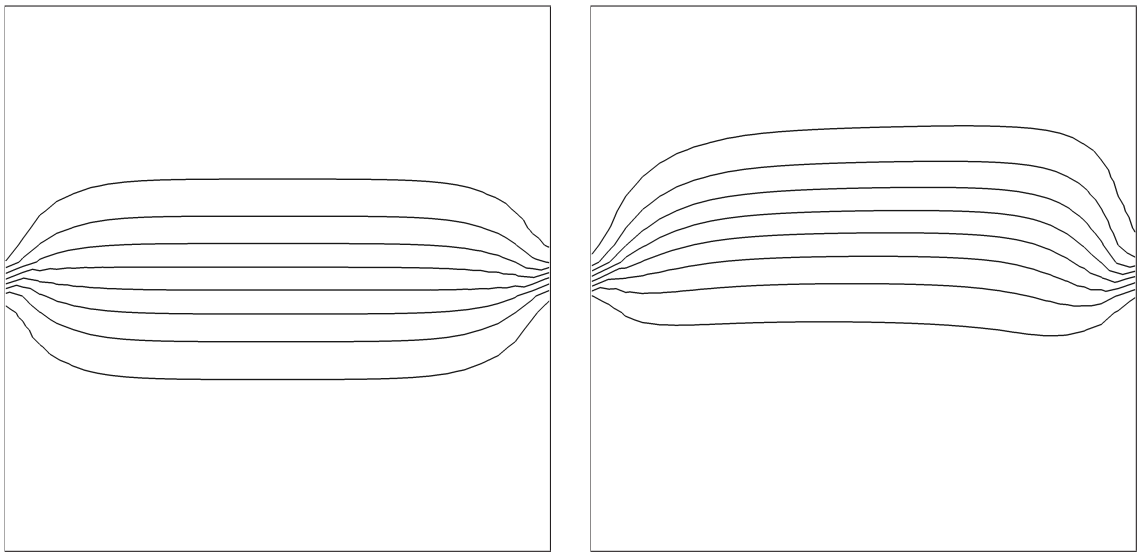

Figure 1: Concentration isolines at the outflow obtained with the nonlinear scheme (left) and with the classical linear approximation of the diffusive flux (right).

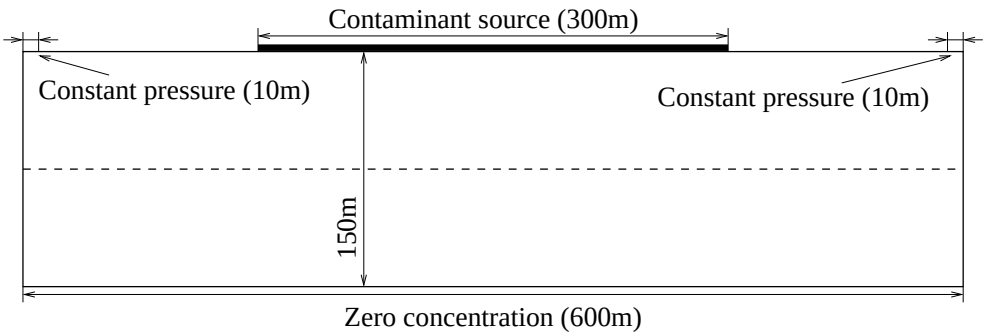

Figure 2: Geometry of Elder problem.

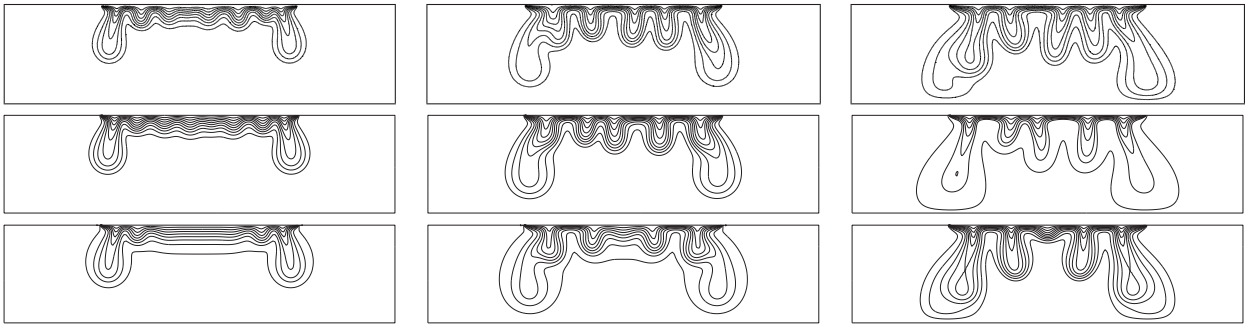

Figure 3: Concentration isolines obtained with the presented scheme (top row), with FEFLOW using unstructured upwind scheme (middle row), and with FEFLOW using Cartesian central scheme (bottom row), after two (left column), three (middle column), and four (right) years.

To be able to compute this two-dimensional problem with a three-dimensional code, we extend the computational domain into the third dimension by introducing thickness 0.8m, and create a tetrahedral grid within this domain. The domain is very thin so that all nodes are at the boundary. A the newly introduced front and the back boundary no-flow condition is set for the pressure and for the concentration.

Elder problem is very sensitive to grid quality and differences in numerical methods. Numerous authors reported qualitatively different solutions. However, some of the reported results do agree on Cartesian meshes [4, 12, 1, 16]. We do not expect our scheme to produce results comparable to these because of the full upwind convective flux discretization and the unstructured meshes. Instead, they will be compared with results obtained with FEFLOW finite element package [8] using full upwind convection discretization and unstructured triangular grids with approximately twice less nodes than in our tetrahedral grid.

Even though Boussinesq approximation is not appropriate for this problem because the density fluctuations are too large [12], results obtained with FEFLOW (see the bottom row of Fig. 3) using Boussinesq approximation, Cartesian mesh, and central convection discretization agree with [4, 12, 1, 16].

Concentration isolines obtained with our scheme using a grid composed of 460,852 tetrahedra are shown in the upper row of Fig. 3. The time step was 500,000 seconds. Iterations were performed until the maximal relative correction of the pressure and the concentration was less then 10^{-8}. Higher accuracy was difficult to reach because the physical problem is unstable. Around 45 iterations were necessary in the developed phases of the computation.

Results obtained with our scheme show similar disagreement with the accurate solution shown in the bottom row of Fig. 3 as the results obtained with another upwind unstructured scheme do (the middle row of Fig. 3). Three-dimensionality of the problem that our code is solving may introduce additional errors.

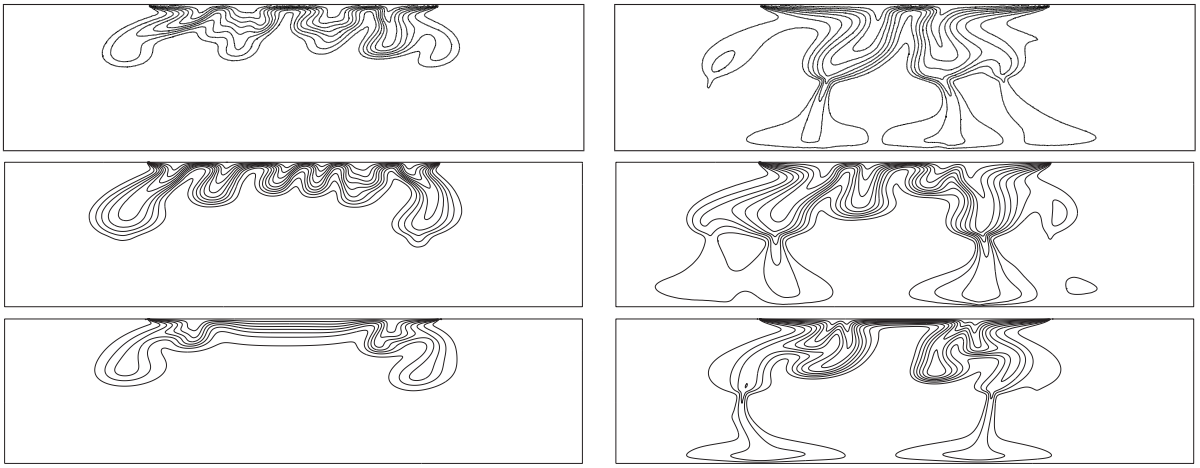

Figure 4: Concentration isolines for the modified anisotropic problem obtained with the presented scheme (top row), with FEFLOW using unstructured upwind scheme (middle row), and with FEFLOW using Cartesian central scheme (bottom row), after one (left) and two (right) years.

In order to test the behavior of the scheme in the case when the permeability tensor is anisotropic and discontinuous, we have modified the Elder problem. We have divided the computational domain in two horizontal layers of equal height, see Fig. 2. Anisotropic tensor

$$\boldsymbol{\kappa}|_{upper} = \mathbf{R}^{-1} \begin{bmatrix} 4.791 \cdot 10^{-12} & 0 \\ 0 & 4.791 \cdot 10^{-13} \end{bmatrix} \mathbf{R}, \qquad \mathbf{R} = \begin{bmatrix} \cos\alpha & \sin\alpha \\ -\sin\alpha & \cos\alpha \end{bmatrix} \tag{28}$$

has been prescribed in the upper layer, where $\alpha = 5\pi/180$, while in the lower layer

$$\boldsymbol{\kappa}|_{lower} = \begin{bmatrix} 1.0194 \cdot 10^{-11} & 0 \\ 0 & 4.791 \cdot 10^{-12} \end{bmatrix}. \tag{29}$$

The permeability in the third direction is taken to be equal to the horizontal permeability of the two-dimensional problem before the rotation, i.e. $4.791 \cdot 10^{-12}$ in the upper part, and $1.0194 \cdot 10^{-11}$ in the lower part. Thickness of the domain in the anisotropic case was 1m, and there were 289,227 tetrahedra. Time step was $100,000$ seconds, and around 110 iterations were needed in each time step to achieve the accuracy of 10^{-6}. Slow convergence in comparison with the isotropic case was also observed with FEFLOW.

Like in the isotropic case, our results disagree with the results obtained with the central Cartesian FEM discretization to a similar extent as the results obtained with the unstructured upwind FEM discretization do (see Fig. 4). However, while FEFLOW gave negative concentrations of more than 10% of the total concentration span in the upwind case and more than 30% in the central case (locally near the two ends of the contaminant source - not visible in Fig. 4), concentration that our code computes is non-negative.

5 DISCUSSION AND CONCLUSIONS

We have presented a monotone non-linear method for the computation of flow and mass transport with the concentration-dependent density. The concentration is guaranteed to be non-negative. However, this does not hold for the pressure. The onset of brines in Example 2 creates the underpressure along the upper boundary which is lower than anywhere at the boundary or inside the domain at the previous time step. Mathematically this is caused by the divergence of the gravity term in (1), (2), which may take any sign.

Atmospheric pressure is usually neglected when computing incompressible flows, because the pressure is determined only up to an additive constant by the flow equations. However, if we set the atmospheric pressure to zero in Example 2, then negative pressure will appear in the domain, and this will break our diffusion scheme, which is unable to cope with negative variables. Therefore we use the physical pressure.

The examples that we presented show that the scheme is considerably more accurate then if the classical finite volume diffusive flux discretization was used, and that it is in line with FEFLOW when full upwind discretization of the convective term is used together with an unstructured grid, except that our scheme does not produce negative concentrations. For our computations of Elder problem to be closer to the best available data, it is necessary to improve the accuracy by using a second-order accurate upwind-biased limited discretization of the convective term such as the one presented in [14].

REFERENCES

[1] Ph. Ackerer, A. Younes, and R. Mose. Modelling variable density flow and solute transport in porous media: 1. numerical model and verification. *Transp. porous media*, 35(3):345–73, 1999.

[2] P. Bastian and S. Lang. Couplex benchmark computations obtained with the software toolbox UG. *Comput. Geosci.*, 8(2):125–147, 1998.

[3] F. Brezzi and M. Fortin. *Mixed and hybrid finite element methods*. Springer-Verlag, New York, 1991.

[4] Peter Frolkovič and Hennie De Schepper. Numerical modelling of convection dominated transport coupled with density driven flow in porous media. *Advances in water resources*, 24:63–72, 2001.

[5] Ph.G. Ciarlet. *The Finite Element Method for Elliptic Problems*. North-Holland, Amsterdam, 1978.

[6] B. Cockburn, G. E. Karniadakis, and C.-W. Shu, editors. *Discontinious Galerkin methods: theory, computation, and applications*. Springer-Verlag, Berlin, 2000.

[7] A.A. Danilov and Yu.V. Vassilevski. A monotone nonlinear finite volume method for diffusion equations on conformal polyhedral meshes. *Russ. J. Numer. Anal. Math. Modelling*, 24(3):207–227, 2009.

[8] H.-J.G. Diersch. *FEFLOW 5.3 user's manual*. WASY GmbH, Berlin, Germany, 2006.

[9] J.W. Elder. Numerical experiments with a free convection in a vertical slot. *J. Fluid Mechanics*, 24:823–843, 1966.

[10] J.W. Elder. Transient convection in a porous medium. *J. Fluid Mechanics*, 27(3):609–623, 1967.

[11] G. Bernard-Michel et al. The Andra Couplex 1 test case: comparisons between finite element, mixed hybrid finite element, and finite volume discretizations. *Comput. Geosci.*, 9(2):187–201, 2004.

[12] Olaf Kolditz, Rainer Ratke, H.-J.G. Diersch, and Werner Zielke. Coupled groundwater flow and transport: 1. verification of variable density flow and transport models. *Advances in water resources*, 21(1):27–46, 1998.

[13] K. Lipnikov, D.Svyatskiy, and Yu.Vassilevski. Interpolation-free monotone finite volume method for diffusion equations on polygonal meshes. *J. Comp. Phys*, 228(3):703–716, 2009.

[14] K. Lipnikov, D.Svyatskiy, and Yu.Vassilevski. A monotone finite volume method for advection-diffusion equations on unstructured polygonal meshes. *J. Comp. Phys.*, 229(11):4017–4032, 2010.

[15] K. Lipnikov, M. Shashkov, D.Svyatskiy, and Yu.Vassilevski. Monotone finite volume schemes for diffusion equations on unstructured triangular and shape-regular polygonal meshes. *J. Comp. Phys*, 227(1):492–512, 2007.

[16] CM. Oldenburg and K. Pruess. Dispersive transport dynamics in a strongly coupled groundwater–brine flow system. *Water Resour. Res.*, 31(4):289–302, 1995.

[17] C. Le Potier. Schema volumes finis monotone pour des operateurs de diffusions fortement anisotropes sur des maillages de triangle non structures. *C.R. Math. Acad. Sci. Paris*, 341:787–792, 2005.

[18] Yu.V. Vassilevski and I.V. Kapyrin. Two splitting schemes for nonstationary convection-diffusion problems on tetrahedral meshes. *Comput. Math. Math. Phys.*, 48(8):1349–1366, 2008.

[19] C.J. Voss and W.R. Souza. Variable density flow and the solute transport simulation of regional aquifers containing a narrow freshwater-saltwater transition zone. *Wat. Res. Res*, 23:1851–1866, 1987.

[20] A. Yuan and Z. Sheng. Monotone finite volume schemes for diffusion equations on polygonal meshes. *J. Comp. Phys.*, 227(12):6288–6312, 2008.